Annual Methodological Archive Research Review
http://amresearchreview.com/index.php/Journal/about
Volume 4, Issue 3 (2026)

Online ISSN 3007-3197
Print ISSN 3007-3189

http://amresearchreview.com/index.php/Journal/about

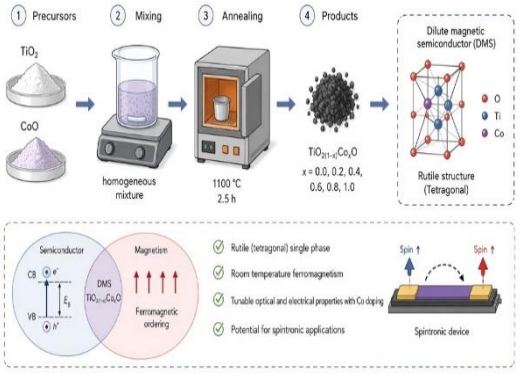
Structural, Optical, and Dielectric Properties of CoO doped TiO_2 for Energy Storage Applications

Sabeeha Ameen[a*] (Corresponding Author), **Madiha Ameen**[b], **Hafiza Bushra Gul**[c], **Liaqat Ali** [d*], **Hafiza Ambreen Gul**[e]

[a] Lahore College for Women University, Lahore, Pakistan.
Email: sabihaameen3@gmail.com
[b] University of Education Lahore, Pakistan
Email: madiaameen111@gmail.com
[c] Islamia College University, Peshawar, Pakistan
Email: hafiza.bushra.gul@gmail.com
[d] Harbin Institute of Technology, Shenzhen, China
Email: 24bf58045@stu.hit.edu.cn
[e] Allama Iqbal Open University, Islamabad, Pakistan
Email: hafiza.ambreen.gul@gmail.com
*Corresponding Author

ABSTRACT

Dilute magnetic semiconductors (DMS) exhibit a unique combination of semi-conductor and magnetic properties. They are composed of a semiconducting matrix that incorporates a small percentage of magnetic cations, specifically transition metals. For functional spintronic devices to be realized, materials that are compatible with current semiconductor materials at operating temperature and possess ferromagnetic ordering are needed. It appears that a dilute magnetic semiconductor is a type of ferromagnetic semiconductor with advantageous experimental properties. CoO-doped titanium dioxide, $TiO_{2(1-x)}Co_xO$ (x=0.0, 0.2, 0.4, 0.6, 0.8 and 1), (DMS) prepared by a physical method at an Annealing temperature of 1100 °C for 2.5 hours. The XRD pattern confirmed the presence of a single-phase rutile. The FT-IR analysis revealed that the vibration bands of the $TiO_{2(1-x)}Co_xO$ semiconductors are in the wavenumber range of 400–4000 cm-1. The grain sizes were measured using a scanning electron microscope (SEM). UV-Vis absorption spectroscopy explains the optical properties of all undoped and doped samples. The magnetic properties of the samples were assessed at room temperature using a Vibrating Sample Magnetometer (VSM), which revealed ferromagnetic characteristics. The electrical conductivity of the doped $TiO_{2(1-x)}Co_xO$ was evaluated through dielectric analysis. Both electrical resistance and bandgap measurements provided further validation of the ferromagnetic behaviour exhibited by the $TiO_{2(1-x)}Co_xO$ series.



Keywords: DMS, rutile, TiO_2, tetragonal, ferromagnetic

Annual Methodological Archive Research Review
http://amresearchreview.com/index.php/Journal/about
Volume 4, Issue 3 (2026)

Online ISSN 3007-3197
Print ISSN 3007-3189

http://amresearchreview.com/index.php/Journal/about

1. Introduction

Semimagnetic semiconductors (SMSs) represent a distinct category of materials that lie at the intersection of semiconductors and magnetic substances. Often referred to as dilute magnetic semiconductors, these materials are essentially semiconductor solid solutions in which certain cation sites are substituted with transition metals or rare-earth elements. Notably, the crystallographic structure of the semiconductor remains intact, and the lattice constant varies as a function of the compositional changes. From a magnetic perspective, SMSs are characterized as disordered magnetic materials due to the random distribution of magnetic atoms within the cation sublattice of the semiconductor compound. [1][2]

These materials are generally composed of semiconducting matrices that incorporate a small percentage of magnetic cations, primarily sourced from transition metal oxides.[3][4][5].

This review has concentrated on the significant advancements in the material research of metallic ferromagnetic (III, Mn)V semiconductors over recent years. The progress achieved in understanding and developing the bulk properties of the (Ga, Mn)As and (In, Mn)As systems in the metallic regime has been substantial. However, numerous challenges persist in other (III, Mn) V-based semiconductors and in lower-dimensional systems, such as digitally doped heterostructures. Continued exploration of both transport and magneto-optical effects presents a promising avenue for further advancements in these materials [6] [7]. Early explorations into the ferromagnetic properties of these semiconductors focused on II-VI and III-V compounds, including manganese-doped CdTe and GaAs. Notably, Ohno demonstrated ferromagnetism in Mn-doped GaAs; however, the observed Curie temperature (Tc) was limited to a modest 110 K. The pioneering work on oxide-based DMS was conducted by Matsumoto et al., who investigated a Co-doped Titanium dioxide (TiO_2) thin film fabricated via pulsed laser deposition (PLD) and molecular beam epitaxy (MBE), achieving a Curie temperature significantly exceeding room temperature[8]. TiO_2, a notable oxide-based material (O-DMS), exhibits a range of intriguing properties that include transparent absorption within the visible light spectrum, an extensive band gap, a high refractive index, and minimal absorption characteristics.[9]. Numerous studies have concentrated on TiO_2 films due to their remarkable optical and electrical characteristics. These include a high dielectric constant, elevated refractive index, substantial band gap, and exceptional transmittance within the visible spectrum [10] [11]. These attributes render TiO_2 a valuable candidate for various applications, including catalysis, photoanodes, solar cells, and magneto-optical technologies. Notably, TiO_2 doped with cobalt (Co) or iron (Fe) exhibits ferromagnetic behavior at room temperature across both the anatase and rutile crystalline forms, with the extent of ferromagnetism highly dependent on the specific concentrations of the dopants used. Furthermore, the magnetic properties observed at room temperature can vary significantly, influenced by the manufacturing processes and growth conditions employed.[12]. Among the transition metal oxides doped, Cobalt oxide (CoO) is an important dopant both theoretically and experimentally because it has a great influence on charge carrier mobility. It appears to be a ferromagnetic dopant in dilute magnetic semiconductors[13]. Significant research has been conducted on TiO_2-based

Annual Methodological Archive Research Review
http://amresearchreview.com/index.php/Journal/about
Volume 4, Issue 3 (2026)

Online ISSN 3007-3197
Print ISSN 3007-3189
http://amresearchreview.com/index.php/Journal/about

dilute magnetic semiconductors (DMS), with a focus on single-transition-metal doping. However, the potential of CoO dopants has not received adequate attention. The incorporation of CoO as a dopant has the potential to enhance the properties of these DMS materials substantially.

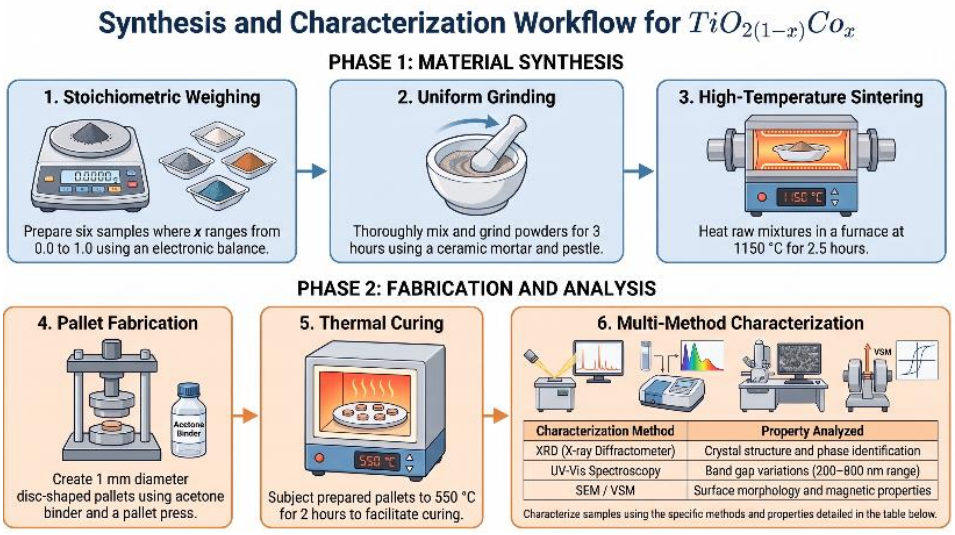
The present work is an experiment in which CoO was used as a dopant in TiO_2. The purpose of doping is to induce ferromagnetism at room temperature and increase the carrier density in TiO_2[14]. This can enhance the magnetic and optical properties, thereby improving efficiency for strain gauge applications [15]. As for now, the dielectric properties of CoO doped TiO_2 have not been investigated. So, in this project, we have focused on dielectric properties in detail.

2. Experimentation

A series of six powder samples characterized by the general formula $TiO_{2(1-x)}Cox$, where x takes on values of 0.0, 0.2, 0.4, 0.6, 0.8, and 1, were synthesized using the powder metallurgy technique. Each sample was carefully weighed according to its stoichiometric proportions using a precise electronic balance. Following this, the individual powder samples were thoroughly mixed and ground for three hours in a ceramic mortar and pestle to ensure a uniform blend. Subsequently, these raw mixtures underwent sintering in a furnace at a temperature of 1150°C for 2.5 hours.

From the synthesized materials, a portion was utilized to fabricate pallets for the assessment of dielectric properties. The Carver pallet press was employed to create disc-shaped pallets with a diameter of 1 mm, using acetone as a binding agent. These prepared pallets were then subjected to a heating process at 550°C for two hours to facilitate curing.

This study involved an examination of the crystal structure and phase identification of the samples utilizing an X-ray diffractometer. Additionally, UV-visible spectroscopy was conducted to investigate variations in the band gap, with optical assessments performed over a wavelength range of 200 to 800 nm. The surface morphology of the samples was analyzed using a scanning electron microscope (SEM), while magnetic properties were evaluated at room temperature through a vibrating sample magnetometer (VSM).



Annual Methodological Archive Research Review
http://amresearchreview.com/index.php/Journal/about
Volume 4, Issue 3 (2026)

Online ISSN 3007-3197
Print ISSN 3007-3189

http://amresearchreview.com/index.php/Journal/about

3. Results and discussion

3.1 XRD ANALYSIS

The X-ray diffraction (XRD) patterns for both undoped and doped TiO_2 nanoparticles are presented in Figure 1. Notably, all observed peaks correspond to the tetragonal rutile phase of TiO_2, characterized by the space group P 42/m, as outlined in JCPDS 96-410-2356. The reflective peaks identified include (111), (101), (120), (211), and (002).

JCPD *(Card #96-410-2356)* confirmed the rutile tetragonal structure of the samples

The values of the lattice constants increased with increasing CoO content. The reason for the reduced lattice constant is attributed to the incorporation of the ionic radii of the dopants Co^{1+} (0.65 Å) and O^{-1} (1.4Å) introduced into the Ti^{4+} (0.74Å) lattice. The unit cell volume of CoO doped TiO_2 remains constant, as shown in the table. The grid parameters a and c are determined by the specified relationship.

$$\frac{1}{d^2} = \frac{h^2+k^2}{a^2} + \frac{l^2}{c^2} \quad \text{.....(1)}$$

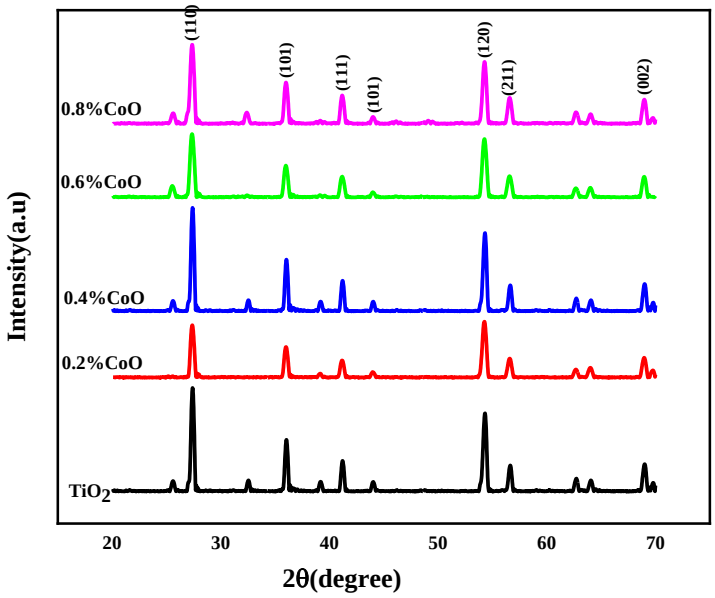


Figure 1: XRD analysis for $TiO_{2\,(1-x)}Co_xO$ rutile phase

Table 1 Lattice parameters of XRD for $TiO_{2\,(1-x)}\,Co_xO$

samples	Crystalline size	a=b	c	Interspacing distance' d	Unit cell $V=a^2c$
Pure TiO_2	31.61	4.59	2.72	3.2524	57.3052
0.2%CoO	28.98	4.60	2.72	3.2547	57.5553
0.4%CoO	21.40	4.60	2.73	3.2547	57.7609
0.6%CoO	20.46	4.62	2.72	3.2695	57.2786
0.8%CoO	18.53	4.59	2.72	3.2525	57.3052

Annual Methodological Archive Research Review
http://amresearchreview.com/index.php/Journal/about
Volume 4, Issue 3 (2026)

Online ISSN 3007-3197
Print ISSN 3007-3189

http://amresearchreview.com/index.php/Journal/about

The crystallite size of the samples with different CoO concentrations was determined using Sharer's formula[16][17].

$$D = \frac{k\lambda}{\beta cos\theta} \text{ .....(2)}$$

The band gap energy and lattice constants increased with increasing CoO content. This is due to the quantum size effect. In this analysis, D represents the crystallite size, k is a constant, and the wavelength employed is 1.54 Å. The full width at half maximum (FWHM) and the angle of reflection are also key parameters in this study. Notably, the CoO-doped TiO_2 exhibits a reduction in crystallite size compared to its pure counterpart. This observed decrease can be attributed to a slight shift in the peak position of the doped samples towards higher angles, which indicates a variation in the lattice constant.

$$L = \left(\frac{a^2}{3} + \left(\frac{1}{2} - \text{U}\right)^2 c^2\right)^{\frac{1}{2}} \text{.....(3)}$$

As the concentration increases, the bond length tends to increase, leading to greater distortion within the crystal structure. Table 2 illustrates that the TiO_2 bond lengths across all samples exhibited a decreasing trend. Additionally, the atomic packing factor (APF) of the nanoparticles was calculated using the following formula:

$$APF = \frac{2\,\pi\,a}{3\sqrt{3}c} \text{.....(4)}$$

The lattice constants are represented by the variables 'a' and 'c'. As shown in Table 2, an upward trend in the Atomic Packing Factor (APF) has been identified. Notably, the APF for pure TiO_2 is approximately 77%

Table 2 XRD Calculated values of the structural parameters of $TiO_{2\,(1-x)}\,Co_xO$

samples	FWHM (nm)	Dislocation density	Ti-O bond	Positional parameters(u)	APF	strain
Pure TiO_2	0.65555	0.217692579	2.890074	1.199219	3.371368	0.0044
0.2%CoO	0.73967	0.192935188	2.898095	1.203359	3.378713	0.0048
0.4%CoO	0.62939	0.226740765	2.89435	1.211667	3.3669	0.0065
0.6%CoO	0.62492	0.228316226	2.914172	1.196388	3.393404	0.0068
0.8%CoO	0.63967	0.192935188	2.890074	1.199219	3.371368	0.0075

Further examination reveals a significant difference in the ionic charges of Co^{2+} and Ti^{4+}, suggesting that the incorporation of cobalt dopants leads to the creation of oxygen vacancies to uphold charge neutrality in the material. Additionally, it is important to highlight that the introduction of the dopant results in a modest increase in the lattice parameter, as detailed in Table 1. This increase aligns with expectations, given that the ionic radius of Ti^{4+} ions (0.74 Å) is larger than that of Co^{2+} ions (0.65 Å).

Annual Methodological Archive Research Review
http://amresearchreview.com/index.php/Journal/about
Volume 4, Issue 3 (2026)

Online ISSN 3007-3197
Print ISSN 3007-3189

http://amresearchreview.com/index.php/Journal/about

The volume of the unit cell can be calculated by the following formula

$$V=\frac{a^2}{c} \quad \ldots\ldots\ldots(5)$$

The unit cell volume of CoO doped TiO_2 increases slightly or almost remains constant, as shown in Table 2.

3.2 FT-IR Spectroscopy Analysis

FT-IR analysis revealed that the vibrational ensembles of the $TiO_{2(1-x)}Co_xO$ semiconductors are in the 400-4000 cm-1 wavenumber range. The rutile phase of the TiO_2 vibrational band is shown in Figure 2. The Ti-O stretching band is represented in this image by the bands at 630 cm^{-1}, 640 cm^{-1}, 663 cm^{-1}, 675 cm^{-1}, 1098 cm^{-1}, and 1198 cm^{-1}. The water-Ti-OH bending modes are shown in the band at 1545 cm^{-1}. The stretching of CO_2 is represented by the band between 2058 cm^{-1} and 2285 cm^{-1}. The band at 3659 cm^{-1} represents the vibrational connection of the O-H hydroxyl groups and can be broken by annealing materials at high temperatures.

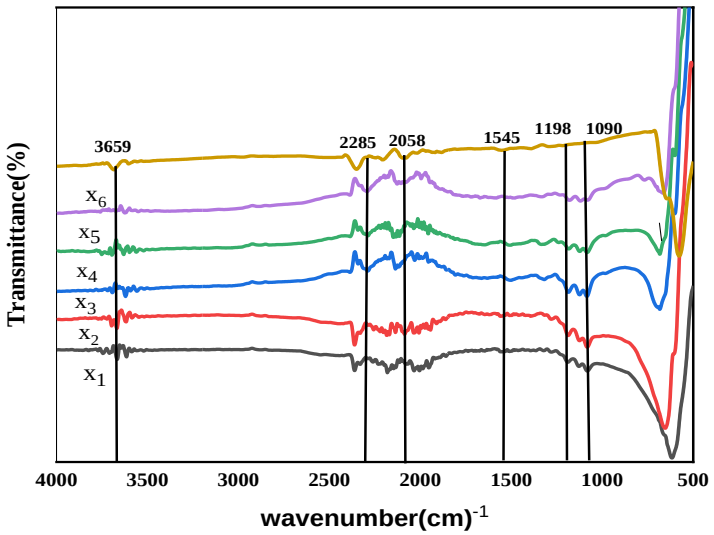


Figure 2: Plot of Transmittance vs. wavenumber for Rutile phase of $TiO_{2\ (1-x)}Co_xO$ (0.00, 0.2, 0.4, 0.6, 0.8, and 1.00)

3.3 SEM

Figure 3 shows the SEM images of each sample in the $TiO_{2(1-x)}CoxO$ series. These micrographs show a tetragonal image that is well defined and has clear boundaries. It can be seen that there are no agglomerates and that the surface morphology is uniform. The average particle sizes were estimated through the application of linear regression analysis on the corresponding plots. The resultant graphs clearly illustrate a trend whereby the particle size exhibits an increase in correlation with the rising doping concentration.

Annual Methodological Archive Research Review
http://amresearchreview.com/index.php/Journal/about
Volume 4, Issue 3 (2026)

Online ISSN 3007-3197
Print ISSN 3007-3189

http://amresearchreview.com/index.php/Journal/about

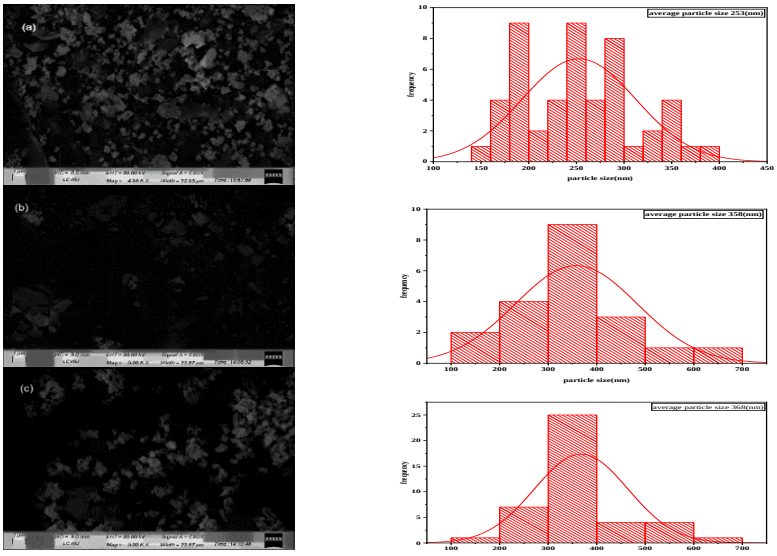


Figure 3: SEM micrographs of $TiO_{2(1-x)}Co_xO$

3.4 UV-visible

The optical properties of CoO-doped TiO_2 nanoparticles were examined through UV-Vis absorption spectroscopy. Our findings indicate that various factors, including oxygen deficiency, particle size, and defects present in the synthesized materials, substantially influence the absorption characteristics observed in these nanoparticles. The absorption edge is in the range of 364–532 nm, as shown in the figure.

The band gap energy of synthesized TiO_2 nanoparticles was estimated using *Tauc's formula*[18].

$$ahv = B(hv - Eg)^{n} \ldots\ldots\ldots (6)$$

Where the absorption wavelength (nm), hv is the energy of the photon, and Eg is the band gap. The plot of ahv vs. $E(eV)$ is shown in Figure 4. The linear part of the plot is extrapolated to determine the bandgap energy values. These results show that the bandgap energy values decrease as the dopant concentration is increased from 0.0 to 1.0%. The values of the direct band gap energy for the rutile phase for a dopant concentration of 0.0-1.0% are given in the table. These results show that the band gap energy values decrease with increasing dopant concentration.

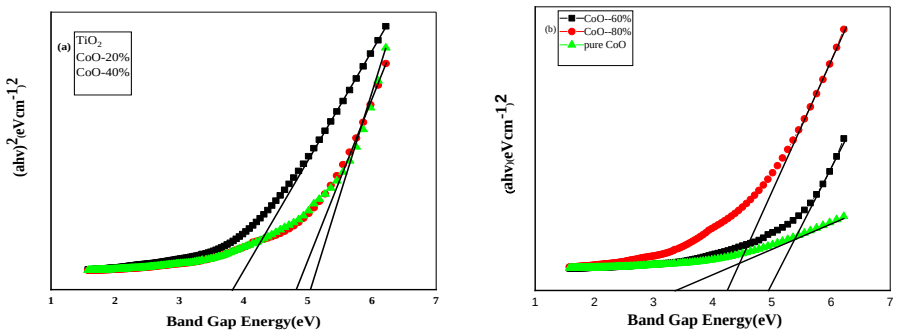


Figure 4 (a), (b) The absorbance versus wavelength plot of rutile phase $TiO_{2(1-x)}Co_xO$.

Annual Methodological Archive Research Review
http://amresearchreview.com/index.php/Journal/about
Volume 4, Issue 3 (2026)

Online ISSN 3007-3197
Print ISSN 3007-3189
http://amresearchreview.com/index.php/Journal/about

These results show that the band gap energy values decrease with increasing dopant concentration. These results differ from the reported band gap energy for the rutile phase, i.e., 3.0-3.16eV. The reason for decreasing energy values with increasing CoO concentration lies in the high concentration of CoO, since the band gap energy of CoO is 2.8 eV and is therefore lower than the band gap energy of TiO_2, i.e, 3.2eV. The reduction in band gap energy can primarily be ascribed to the interaction occurring between the localized d electrons of Co^{2+}ions, which replace Ti^{4+}ions, and the conduction band electrons of TiO_2. In the Co-doped TiO_2 sample, the substitution of $Co^{2+}$for Ti^{4+}induces a substantial crystal field effect due to the influence of adjacent oxygen ions. This pronounced crystal field interaction results in the splitting of the D-band states of Co^{2+} into distinct ground and excited states. Consequently, the splitting phenomenon facilitates d-d electronic transitions within the visible spectrum.[19].

3.5 Dielectric properties measurements

The dielectric characteristics of nanoparticles are influenced by several factors, including lattice parameters, temperature, and frequency. The dielectric constant can be expressed by the equation:

$$\epsilon = C_p\, d / \epsilon_o\, A \quad \text{.....(7)}$$

In this formula, C_p denotes the capacitance of the sample in Farads (F), d represents the thickness of the pellet, ε_0 signifies the permittivity of free space, and A is the cross-sectional area of the circular pellet. The conductivity is determined by the given formula

$$\sigma = \varepsilon'\, \varepsilon_0\, \omega \tan\delta \quad \text{.....(8)}$$

The dielectric loss is determined by the given formula

$$\tan\delta = 1/2\pi f\, \varepsilon' \varepsilon_0 \rho \quad \text{.....(9)}$$

3.5.1 Dielectric constant variations with frequency

The variation of the dielectric constant with increasing frequency for $TiO_{2(1-x)}CoO$ nanoparticles has been studied and shown in Figure 5.1. The dielectric constant of the prepared nanoparticles is plotted for various Fe concentrations of 0.00, 0.2, 0.4, 0.6, 0.8, and 1.00. It has been noted that the dielectric constant exhibits an increase at low frequencies, but as the frequency rises, a subsequent decrease in the dielectric constant is observed. At very high frequencies, this value approaches a steady state, largely attributed to contributions from dipolar, ionic, space charge, and electronic polarization mechanisms.

Annual Methodological Archive Research Review
http://amresearchreview.com/index.php/Journal/about
Volume 4, Issue 3 (2026)

Online ISSN 3007-3197
Print ISSN 3007-3189

http://amresearchreview.com/index.php/Journal/about

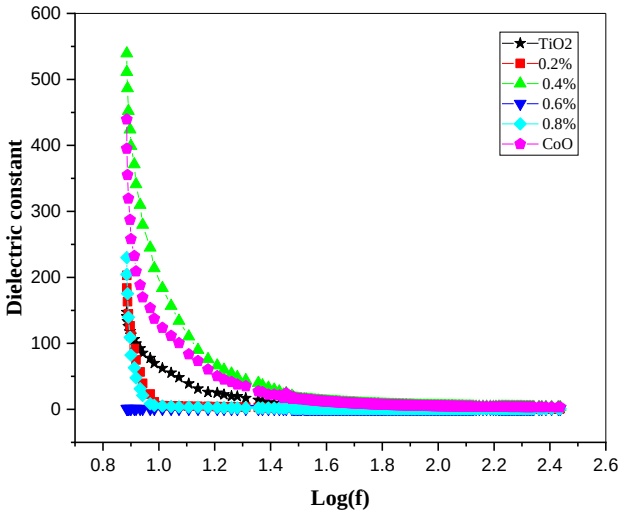


Figure 5.1 graph between dielectric constant and *log f*

3.5.2 Tan loss variations with frequency

The variation of the dielectric loss with increasing frequency for $TiO_{2(1-x)}Co_xO$ has been studied and shown in the Figure 5.2. It has been observed that the dielectric loss decreases with increasing frequency. At low frequencies, there are high dielectric losses due to space charge polarization, which may be due to the inhomogeneity of the structure of the dielectric material used. Space charge polarization occurs when the externally applied electric field shifts the space charges and creates dipoles. It is observed that the dielectric constant remains constant at higher concentrations of Co^{2+}.

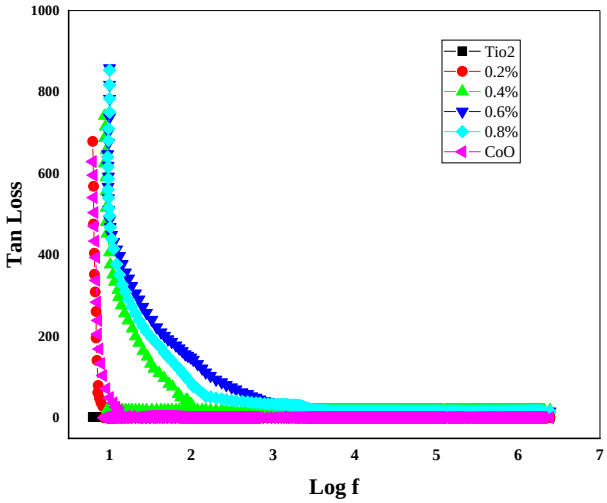


Figure 5.2 Plot of tan loss vs. log f

Annual Methodological Archive Research Review
http://amresearchreview.com/index.php/Journal/about
Volume 4, Issue 3 (2026)

Online ISSN 3007-3197
Print ISSN 3007-3189

http://amresearchreview.com/index.php/Journal/about

3.5.3 Dielectric constant variations with frequency

The variation in conductivity with increasing frequency for $TiO_{2(1-x)}Co_xO$ was studied and shown in the Figure 5.3. The electron jumping mechanism creates the AC conductivity. It has been observed that AC conductivity increases with high frequency because electrons migrate with increasing frequency. In the case of CoO-doped TiO_2, the AC conductivity depends on hopping for a charge rate between Ti^{2+}, Ti^{3+}, and Ti^{4+} because electrons migrate with increasing frequency.

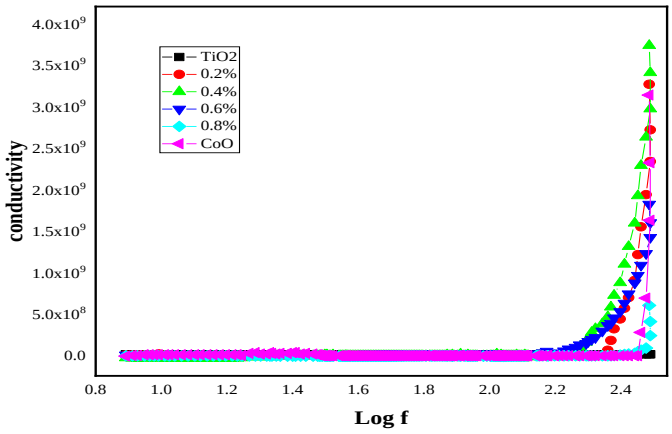


Figure 5.3 graph between conductivity and *log f*

3.6 Vibrating Sample Magnetometer

The magnetic behaviour of $TiO_{2(1-x)}Co_xO$ (x=0.0-0.8) nanoparticles is studied by vibration of the sample magnetometer. The samples with cobalt oxide concentrations of 0.0, 0.2, 0.4, 0.6, 0.11, and 0.8 (wt%) doped in TiO_2 were prepared by the solid-state method at room temperature. The samples were annealed at 1100°C to obtain the rutile phase. Figure 5.4 shows the room-temperature ferromagnetism for undoped and CoO-doped TiO_2 nanoparticles of the rutile phase of TiO_2[20]. The findings indicate that both remnant and saturation magnetization exhibit an increase as the concentration of the dopant is elevated from 0.00 to 0.8% [21]. Prior studies have demonstrated that TiO_2 doped with transition metals displays ferromagnetism at room temperature. This phenomenon can be attributed to the exchange interaction occurring between holes that are trapped in the oxygen 2p orbitals adjacent to the doping site, which substitutes Ti^{4+}ions [23]. Therefore, it is anticipated that as the dopant concentration rises, the magnetization of the TiO_2 host will correspondingly increase. These results corroborate existing literature that suggests a rise in both saturation and remanence with higher levels of dopant concentration [24]. A key factor contributing to the enhanced magnetization is the larger ionic radius of cobalt compared to that of TiO_2. Therefore, as the concentration of cobalt oxide increases, the magnetization also increases [25].

Annual Methodological Archive Research Review
http://amresearchreview.com/index.php/Journal/about
Volume 4, Issue 3 (2026)

Online ISSN 3007-3197
Print ISSN 3007-3189

http://amresearchreview.com/index.php/Journal/about

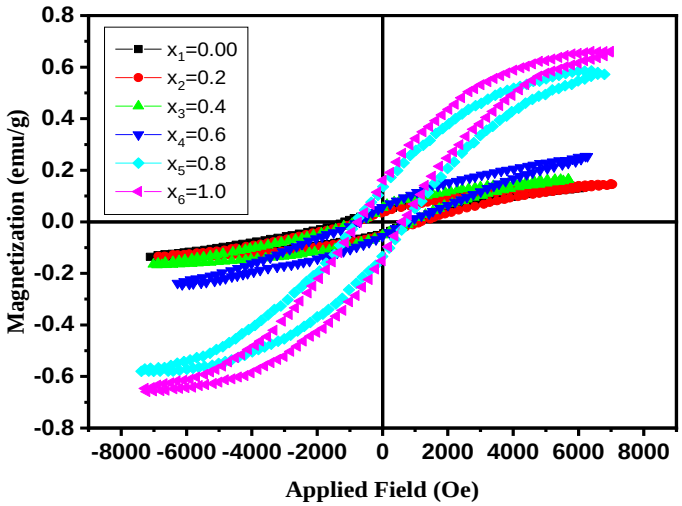


Figure 5.4: Graph between applied field and magnetization

4. Conclusions

An investigation was conducted to synthesize $TiO_{2(1-x)}Co_xO$ (where x ranges from 0.0 to 0.8) as a diluted magnetic semiconductor (DMS) via the powder metallurgy method. Structural analyses demonstrated the successful formation of the rutile phase of TiO_2. Room-temperature magnetic measurements indicated the presence of ferromagnetism across all concentrations of CoO. Additionally, the resistivity measurements, along with UV-Visible analysis, confirmed that the synthesized series of $TiO_{2(1-x)}Co_xO$ (x=0.0-0.8) falls within the semiconducting range. Our findings indicate that this series exhibits ferromagnetic properties, positioning it as a notable DMS.

Data Availability Statement: The data presented in this study are available on request from the corresponding authors

Conflicts of Interest: The authors declare no conflicts of interest.

Reference

1. A.G.U. Perera, G. Ariyawansa, S.G. Matsik Terahertz Detection Devices, Comprehensive Semiconductor Science and Technology Volume 6, 2011, Pages 265-307.
2. A.G.U. Perera, G. Ariyawansa Materials Science and Materials Engineering, 2016. Reference Module in Materials Science and Materials Engineering
3. Baig N, Kammakam I, Falath W, Kammakam I (2021) Nanomaterials: A review of synthesis methods, properties, recent progress, and challenges. Mater Adv 2:1821 1871. https://doi.org/10.1039/d0ma00807a
4. Adeniyi FI, Ogundiran MB, Hemalatha T, Hanumantrai BB (2020) Characterization of raw and thermally treated Nigerian kaolinite-containing clays using instrumental techniques. SN Appl Sci 2:1 14.

Online ISSN 3007-3197
Print ISSN 3007-3189

https://doi.org/10.1007/s42452-020-2610-x

5. Mugundan S, Rajamannan B, Viruthagiri G, et al (2015). Synthesis and characterization of undoped and cobalt-doped TiO2 nanoparticles via sol–sol-gel technique. Appl Nanosci 5:449–456. https://doi.org/10.1007/s13204-014-0337-y
6. Albert, R. , & Barabasi, A. L. (2002). 2002): "statistical mechanics of complex networks. Reviews of Modern Physics, 26(1)
7. M. Bououdina, Y. Song, S. Azzaza. Nano-Structured Diluted Magnetic Semiconductors Reference Module in Materials Science and Materials Engineering 2016
8. Alsulami QA, Rajeh A (2021) Synthesis of the SWCNTs/TiO2 nanostructure and its effect study on the thermal, optical, and conductivity properties of the CMC/PEO blend. Results Phys 28:104675. https://doi.org/10.1016/j.rinp.2021.104675
9. Filippatos PP, Kelaidis N, Vasilopoulou M, et al (2021). Structural, electronic, and optical properties of group 6 doped anatase tio2: A theoretical approach. Appl Sci 11:1–13. https://doi.org/10.3390/app11041657
10. T. Fuyuki, H. Matsunami. Electronic properties of the interface between Si and TiO2 deposited at very low temperatures. Applied Phys, 25 (1986), p. 1288
11. J.-Y. Gan, Y. Chang, T. Wu Dielectric property of (TiO2) x-(Ta2O5) 1-x thin films Appl Phys Lett, 72 (1998)
12. L. Miao, et al. Preparation and characterization of polycrystalline anatase and rutile TiO2 thin films by rf magnetron sputtering Appl Surf Sci, 212 (2003)
13. Challa Gebremichael Gurmessa (2017) Diluted Magnetic Semiconductors (DMSs) and Their Applications
14. Parveen B, Mahmood-ul-Hassan, Khalid Z, et al (2017) Room-temperature ferromagnetism in Ni-doped TiO2 diluted magnetic semiconductor thin films. J Appl Res Technol 15:132 139. https://doi.org/10.1016/j.jart.2017.01.009
15. Waseem S, Anjum S, Mustafa L, et al (2016) Absence of room temperature ferromagnetism in Co and Cr Co-doped TiO2-based dilute magnetic semiconductors. Dig J Nanomater Biostructures 11:411 418
16. Zimou J, Nouneh K, Hsissou R, et al (2021). Structural, morphological, optical, and electrochemical properties of Co-doped CeO2 thin films. Mater Sci Semicond Process 135:106049. https://doi.org/10.1016/j.mssp.2021.106049
17. S. Amer M, A. Ghanem M, Arunachalam P, et al (2019). Modification of mesoporous titanium dioxide with cobalt oxide electrocatalyst for enhanced oxygen evolution reaction. Adv Mater Lett 10:136 144.https://doi.org/10.5185/amlett.2019.2139
18. Swart, S. S. Jai Prakash * , Samriti. Ajay Kumar, Hongliu Dai, Bruno C. Janegitz d, Venkata Krishnan b, Hendrik C. Swart e, Shuhui Sun Materials Today Sustainability Received 11 November 2020 Received in revised form 31 March 2021 Accepted 3 April 2021 Available online 20 April 2021
19. Guskos N, Zolnierkiewicz G, Guskos A, et al (2015) Magnetic resonance study of co-modified (Co, N)-TiO2 nanocomposites. Nukleonika 60:411-416. https://doi.org/10.1515/nuka-2015-0073
20. Mahal HS, Singh BP, Kant R (2021) The effect of Co doping on structural, optical, and dielectric behaviour of TiO2 nanoparticles. Def Sci J 71:390–394.

Online ISSN 3007-3197
Print ISSN 3007-3189

https://doi.org/10.14429/DSJ.71.16720
21. Sharma A, Lee BK (2016) Rapid photo-degradation of 2-chlorophenol under visible light irradiation using cobalt oxide-loaded TiO2/reduced graphene oxide nanocomposite from aqueous media. J Environ Manage 165:1–10. https://doi.org/10.1016/j.jenvman.2015.09.013
22. Qana A. Alsulami, Qana A. (2021). A. Rajeh results of physics, Volume 28, (September) 2021, p. 104675(30)
23. Dai Q, Tang J (2013) The optical and magnetic properties of CoO and Co nanocrystals prepared by a facile technique. Nanoscale 5:7512–7519. https://doi.org/10.1039/c3nr01971c
24. Dutt, V. V., & Dubey, R. S. (2017). Materials Science & Engineering Journal, 9(1).(32)
25. Ali, T., Ahmed, A., & , Tripathi, P.Naseem siddique, M., & Tripathi, P. (2018). Enhanced dielectric properties of Fe-substituted TiO2 nanoparticles. Physica . Part B: Condensed Matter, 534, 1-–4. doi:10.1016/j.physb.2018.01.009.(46)